A compact, active hyperspectral imaging system for the detection of concealed targets

Bernadette Johnson*, Rose Joseph, Melissa Nischan, Amy Newbury, John Kerekes, Herb Barclay, Berton Willard, John J. Zayhowski

MIT Lincoln Laboratory, 244 Wood St., Lexington, MA 02420-9185

ABSTRACT

We have recently conducted a series of laboratory and field tests to demonstrate the utility of combining active illumination with hyperspectral imaging for the detection of concealed targets in natural terrain. The active illuminator, developed at MIT Lincoln Laboratory, is a novel microlaser-pumped fiber Raman source that provides high-brightness, subnanosecond-pulse-length output spanning the visible through near-infrared spectral range. The hyperspectral-imaging system is comprised of a compact, grating-based spectrometer that uses a gateable, intensified CCD array as the detector element. The illuminator and hyperspectral imaging system are mounted on a small platform that is itself mounted on a tripod and scanned in azimuth to build an image scene of up to several hundred spectral bands. The system has been deployed under a variety of environmental conditions, including night-time illumination, and on a variety of target scenes, including exposed and concealed plastic and metallic mine-like targets. Targets have been detected and identified on the basis of spectral reflectance, fluorescence signatures, degree of polarization, and range-to-target information (via range gating). The combination of laser-like broadband illumination and hyperspectral imaging offers great promise in concealed or obscured target detection. Ongoing developments include the incorporation of broadband illuminators in the 1 to 2 μm and 3 to 5 μm spectral bands, with corresponding increases in spectral coverage of the imaging and detection systems.

Keywords: Hyperspectral imaging, laser illumination, landmine detection, target discrimination, fiber Raman laser

1. INTRODUCTION

In recent years, hyperspectral imaging (HSI) has emerged as a tool for applications as diverse as terrain and vegetation characterization, target discrimination, and even non-invasive medical-imaging spectroscopy. In hyperspectral imaging, radiation from a broadband source (typically the sun, but also lamps) is reflected from a target and analyzed in hundreds of spectral bands from the ultraviolet through mid-wave infrared regions. By exploiting the often subtle variations in spectral reflectance, hyperspectral imaging can provide a means of classifying and identifying different elements of a scene that normally, in standard three-color imagery, appear indistinguishable. Despite its proven utility in remote sensing, hyperspectral imaging suffers from some limitations that can restrict its utility in certain other applications. First, typical systems that operate outdoors from either ground-based or airborne platforms require sunshine for the illumination, thus they are restricted to daytime, fair-weather operation. Second, even during daylight, the reflected spectrum is influenced by the angles between the sun, target, and imaging system, which confers an additional level of complexity to the scene analysis. Third, there is a dearth of HSI phenomenology data on potential target classes of interest. If HSI is to realize its full potential as a sensing tool, these limitations must be addressed.

At MIT Lincoln Laboratory, we are exploring the utility of combining laser and laser-like illumination with compact hyperspectral imagers for a variety of applications, including landmine detection. By providing a high-brightness source of illumination, we can operate day or night, under even adverse weather conditions. By collocating that source with the hyperspectral imager, we can eliminate the reflected-signal dependence on solar angle and greatly reduce the effects of solar shadowing on scene interpretation. Finally, by offering a robust illumination source whose output spectrum is well-matched to the detection bands of the HSI, we have developed a capable tool for the exploration of active HSI phenomenology.

The system described in this paper operates in the visible/NIR spectral regions (532 to 900 nm). We are currently expanding the capabilities of this baseline system to include both illumination and imaging capabilities in the 1 to 2 μm and 3

* Correspondence: E-mail: bernadette@ll.mit.edu; Telephone: 781-981-7944

Part of the SPIE Conference on Detection and Remediation Technologies for Mines and Minelike Targets IV • Orlando, Florida • April 1999
SPIE Vol. 3710 • 0277-786X/99/$10.00

to 5 μm spectral regions. Eventually, we intend to incorporate both passive and active imaging from the visible through the long-wave infrared regions, along with the requisite fusion algorithms to exploit the full capabilities of such extended coverage. Applications for this technology include detection and identification of concealed or obscured targets, such as landmines and camouflage paint or fabric, search and rescue, and general enhanced vision aids to vehicle or airplane operators.

2. ACTIVE HYPERSPECTRAL IMAGING SYSTEM BASELINE COMPONENTS

The Active HSI (AHSI) baseline system comprises an illuminator and imaging spectrometer on a tripod-mounted scanning platform, which moves in azimuth as reflected data are acquired (see Figure 1). The illuminator beam shape is a vertical stripe whose divergence is chosen so that the illuminated target area is matched to the instantaneous field-of-view of the imager, determined by the entrance slit of the spectrometer. Light dispersed by the spectrometer is incident on a two-dimensional focal-plane array; thus, at each scan position, a column of spatial data is acquired with full spectral dispersion of each pixel in the column. A scene is built up by scanning the platform azimuthally, which results in a "hypercube" of data comprising one spectral and two spatial dimensions. The hypercube is processed to provide scene classifications, detect anomalies, or identify specific targets, depending on the application. In the following subsections, the hardware components and processing are described in greater detail.

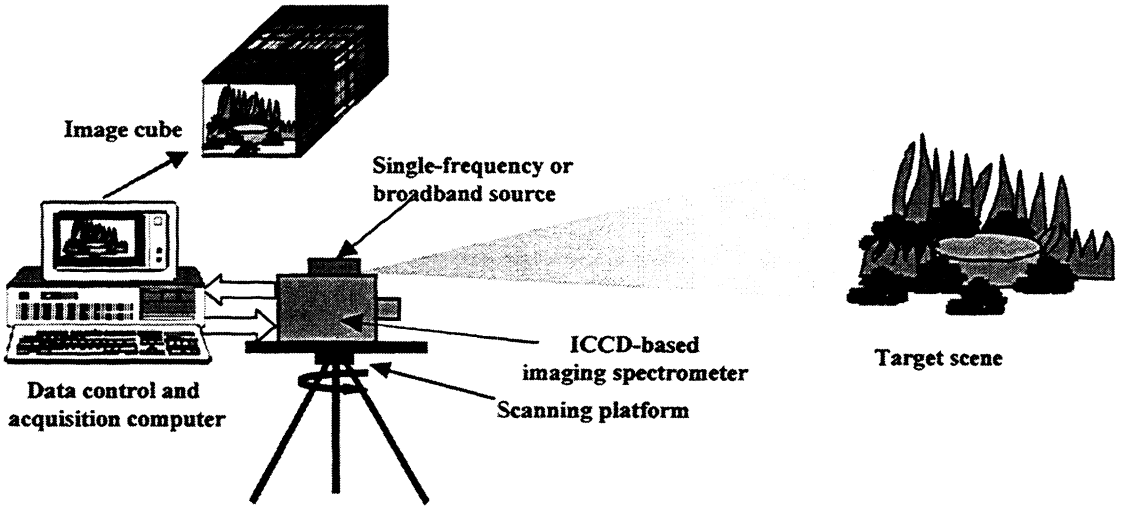

Figure 1: Schematic diagram of the primary components of the active HSI baseline system.

2.1. The Illuminator

We have developed a compact laser-based illuminator that can operate in either of two modes. In the first mode, output from a 532-nm diode-pumped microlaser is shaped by cylindrical optics into a stripe-like beam and incident on a target scene. The 532-nm microlaser is pumped by a 3-W near-infrared diode laser (808 nm) that is coupled to the microlaser by a 1-meter length of optical fiber. The microlaser is passively Q-switched to produce short (of the order of 400 psec) pulses at high repetition rates (up to 16 kHz) with approximately 5 to 8 μJ of per-pulse energy.[1-2] The linearly-polarized 532-nm output is used to examine the degree of polarization of a target scene, which is useful for distinguishing manmade from naturally-occurring objects. It is also used to explore fluorescence imagery, which can be useful in distinguishing vegetation (by chlorophyll fluorescence) and other fluorescing scene components (minerals, certain plastics, etc.).

In the second mode of operation, the 532-nm radiation is focused into a single-mode silica fiber (core diameter ~ 6 μm) of approximately 100 meters in length. Intensities greater than 10 GW/cm^2 are achieved in the fiber core and, within a few meters of propagation, a Stokes-shifted stimulated Raman scattering (SRS) pulse is generated. This pulse, which occurs at 440 cm^{-1} from the 532-nm radiation, is spectrally broadened due to the inherently large Raman gain bandwidth (~40 THz) of silica fibers. This first Stokes-shifted pulse induces a second-order SRS pulse, which is even further broadened and which

pumps higher-order Stokes shifts. After 8 to 10 Raman shifts, the pulses are sufficiently broadened that they overlap to form a continuum, which, for our fiber length, extends from about 680 nm to 900 nm (see Figure 2). The energy conversion from the input 532-nm beam to the output "white-light" beam is between 10 and 15 %, and the high- repetition rate and short-pulse structure of the input beam are preserved. The output radiation is, as with the 532-nm beam, shaped into a stripe that illuminates the target and is imaged by the spectrometer. In summary, the illuminator provides a compact source (the 100m fiber length can be very thinly coiled) of broadband, high-brightness, short-pulse radiation that is not only well-matched (spectrally) to the imaging system, but that is suitable for range-gating.

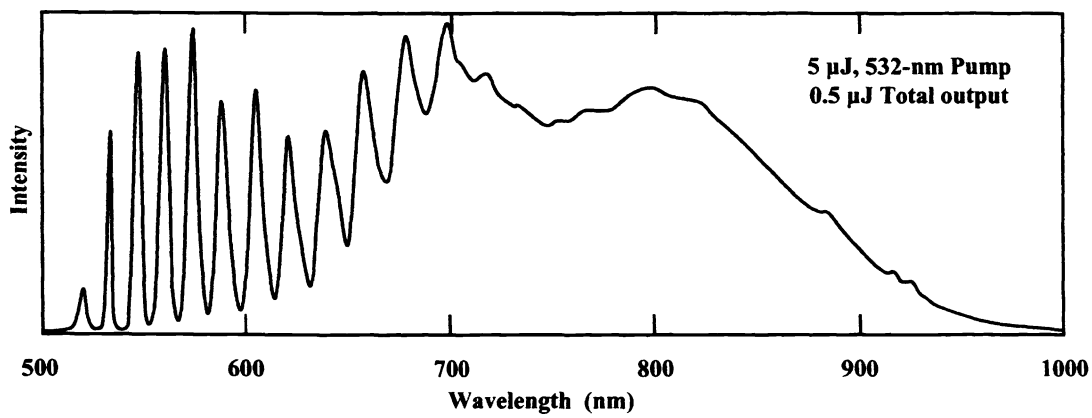

Figure 2: Output spectrum of the 532-nm-pumped broadband illuminator.

2.2. The Imaging Spectrometer

The reflected radiation is imaged onto the entrance slit of a 1/8-meter Acton Research Spectrograph with a 4-inch diameter standard zoom camera lens. The spectrograph has a f/number of approximately 4 and disperses radiation by reflection off of a grating that covers the spectral range of 300 to 1100 nm, with approximately 3 nm spectral resolution at the focal-plane array. For higher-resolution spectral information, we can use a second grating that has 250 nm of total coverage, with sub-nanometer resolution. Although the spectrograph permits f/4 imaging, we typically operate at f/8 or even f/16 to optimize the image quality across the entire focal-plane array.

2.3. The Focal-Plane Array

We use a Princeton Instruments 330 x 1100 CCD array as the imaging spectrometer's detection element. The back-illuminated CCD has a quantum efficiency greater than 60% throughout the visible spectral region, with approximately 25 noise electrons at a 1 Mpixel/sec readout rate. In order to both enhance the signal strength and enable range gating, we can use the CCD with a lens-coupled Gen II image intensifier, optimized for performance from the visible through near-infrared. The Gen II suffers a reduction in pixel resolution of approximately a factor of three from the bare CCD array, but was chosen because it enables gating as fast as 5 nsec. Since our laser pulse lengths are less than 1 nsec, the intensifier gate width represents the shortest-range gate that we can employ. In operation, this means that we can examine the reflected signal from an approximately 75-cm slice in range; this level of range-gating is especially useful in reducing the noise contribution from foreground scatter that can plague images in hazy or smoky environments. The length and initiation of the range gate is controlled by a Princeton Instruments PG-200 programmable gate pulse generator, which can be triggered by the firing of the laser pulse or by an external signal from the controlling computer.

2.4. Data Acquisition and Processing

In the standard mode of operation, a given target scene is imaged four times in succession, acquiring white-light reflectance, fluorescence, and two orthogonal polarization image cubes. The scanning platform has excellent mechanical stability so cube-to-cube image registration is straightforward. The frequency content and the spatial variation of the illuminator are measured by acquiring a hypercube using a high-reflectance Spectralon panel as the target. (Spectralon has a reflectance of almost 99% over the spectral range of interest and is an approximately Lambertian scatterer.) Acquired raw data are corrected for detector nonuniformity and background, and, typically, binned to 10-nm bands. After binning, the

white-light hyperspectral data are normalized to the Spectralon-acquired hypercube, primarily to remove any variations in illuminator intensity across the target scene. The resultant normalized data are processed by a number of algorithms that act, depending on the application, to find targets whose reflectance spectra match those stored in a library, detect scene anomalies, or classify scene components. ENVI (Environment for Visualization of Imagery), an image display and analysis package developed by Research Systems, Inc., is used to manipulate and analyze the data hypercubes. As a final processing step, spatial filtering is frequently employed to search for targets in a specific size category or to reject isolated single-pixel false detections. A diagram of the acquisition and processing architecture is shown in Figure 3.

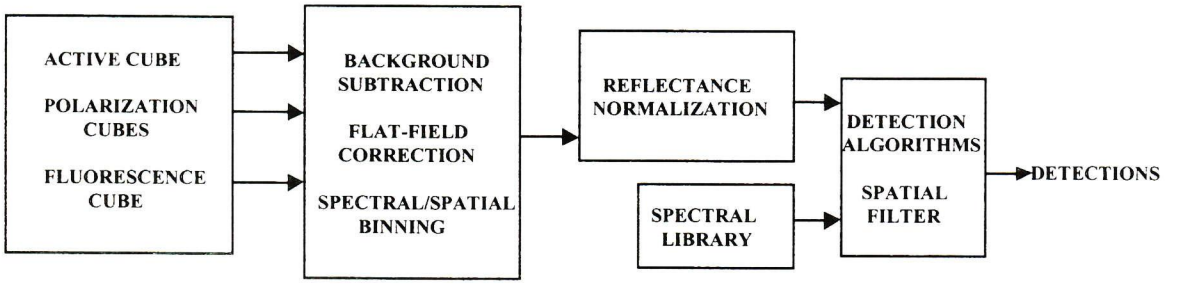

Figure 3: Schematic diagram of formation and analyses of data hypercubes. Resultant processed data is displayed to the operator in color, with specific targets or scene components visually highlighted.

3. EXAMPLES OF BASELINE-SYSTEM MEASUREMENTS

3.1 Target Scene

An example of a laboratory scene containing plastic and metal is shown in Figure 4. The target objects include pieces of green and black plastic, an optical taggant (a brightly colored plastic disk impregnated with a fluorescing dye), a metal wire, and a shell casing. All of the objects were partially concealed by grass and weeds in a natural setting that also included soil and rocks. In the background at the top of the image is a green-painted aluminum panel. Typical operating parameters for this scene are summarized in Table 1; note that no illumination other than that provided by the single-frequency and broadband lasers was used.

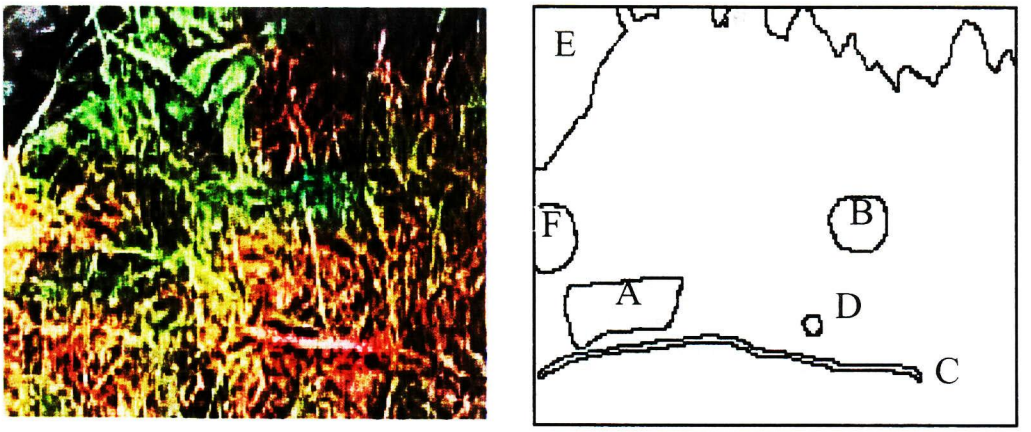

Figure 4: Laboratory target scene containing soil, grass, weeds, partially-obscured plastic and metal objects:
A: Dark-green plastic, B: Bright-green plastic, C: Wire, D: Shell casing, E: Green paint, F: Taggant.

Range	10 meters
Background	Dark room
Illuminator	Fluorescence imaging: 532 nm, 6.7 μJ/pulse, 16 kHz pulse repetition rate Reflectance imaging: white-light source, ~1 μJ/pulse, 16 kHz pulse repetition rate
Integration time	1 second, ungated CCD
Image size	140 pixels (vertical) x 200 frames (in scan direction)
Grating	150 g/mm blazed at 500 nm
Spectral resolution	3-nm FWHM
Spatial resolution	1.25 mm
F/#	16
Binning	10 nm
Spectral coverage	33 white light bands (600-920 nm) 33 fluorescence bands (600-920 nm) 2 polarization bands (horizontal and vertical, 532 nm)

Table 1: Measurement parameters for the scene in Figure 4.

3.2 Fluorescence Imaging

Chlorophyll in vegetation fluoresces at 690 nm and (often) 740 nm when excited by light of a shorter wavelength. As a result, fluorescence imaging can be used to discriminate between live vegetation and green camouflage or other materials. Similarly, certain materials fluoresce, for example, polyesters, some rocks and minerals, and dyed plastics. The scene shown in Figure 4 was imaged at 10-m range using 532-nm active illumination having an average intensity at the target plane of 4 mW/cm^2. This brightness saturates the detector array in the 532-nm wavelength band and offers little contrast information. Figure 5, however, displays two images, one at a band centered at 690 nm, where chlorophyll fluoresces, and one centered at 600 nm, which corresponds to the peak of the optical taggant emission line. Note the readily discernible grass in the former image and the taggant in the latter; these images were derived with very little post-processing (simple thresholding) and illustrate the utility of using fluorescence to classify scene components.

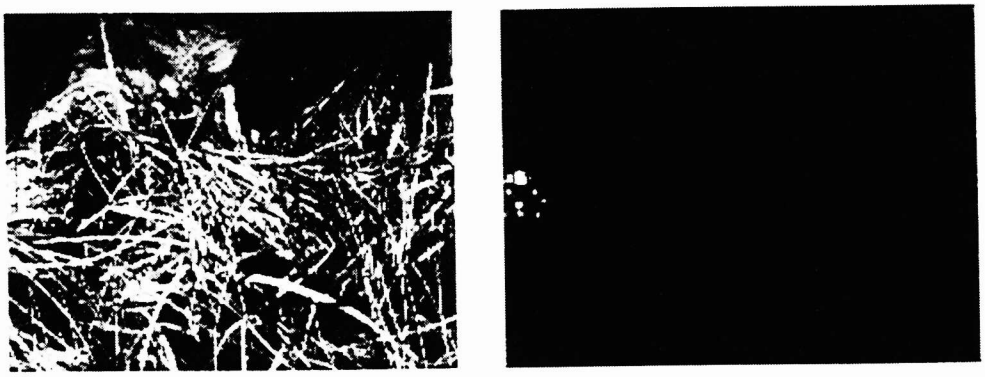

Figure 5: 690-nm chlorophyll fluorescence (left) and 600-nm optical taggant emission (right).

3.3 Polarization Imaging

Naturally-occurring objects such as grass, soil, and other rough surfaces tend to depolarize incident light more than smoother man-made objects. Thus, polarimetry can provide an additional discriminant useful in distinguishing manmade objects in a natural cluttered background. The same scene shown in Figure 4 was illuminated with vertically polarized 532-nm light and imaged through a polarizing film placed in front of the spectrometer. The first image shown in Figure 6 displays the reflected vertical (V) polarization component (transmit axis of the polarizer aligned with polarization vector of the outgoing laser beam). The second image displays the horizontal (H) polarization component, where the polarizer was rotated 90°. The degree of polarization (DOP) is defined as the ratio of the difference to the sum of two orthogonal polarization measurements, DOP=(V-H)/(V+H). The average DOP for the metal objects in the scene was greater than 0.3 while the average background clutter DOP was less than 0.2. Thresholding the DOP image at 0.28 and applying a median filter resulted in the detections shown in the final image in Figure 6.

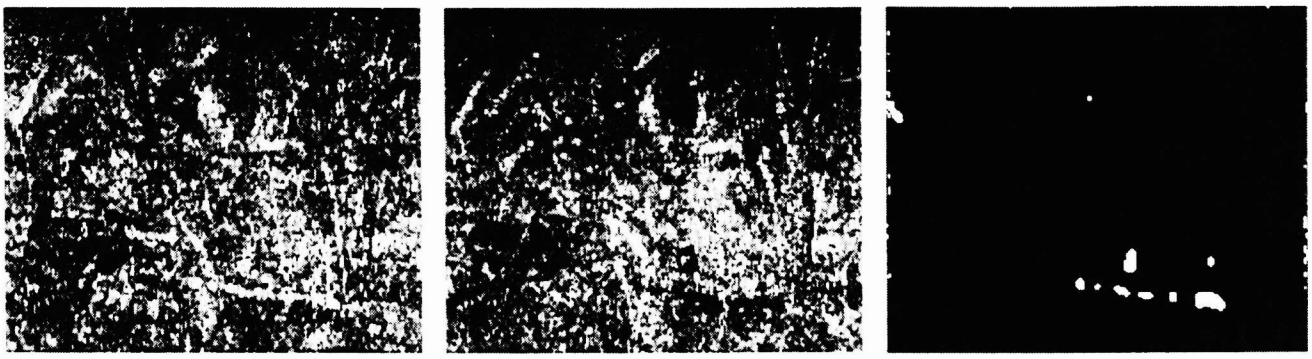

Figure 6: Vertical polarization image at 532 nm (left), horizontal polarization image at 532 nm (center), and processed detections from polarimetric imaging (right).

3.3 Reflectance Imaging

The laboratory scene discussed in the previous subsections was again imaged in a dark room using the white-light illuminator. Figure 7 displays the reflectance spectra for several of the scene components described in Figure 4. Since all of these scene components are green in hue, their reflectance spectra are similar in the visible portion of the spectrum. However, at wavelengths greater than about 700 nm, their spectra diverge sufficiently to permit discrimination between target objects and background.

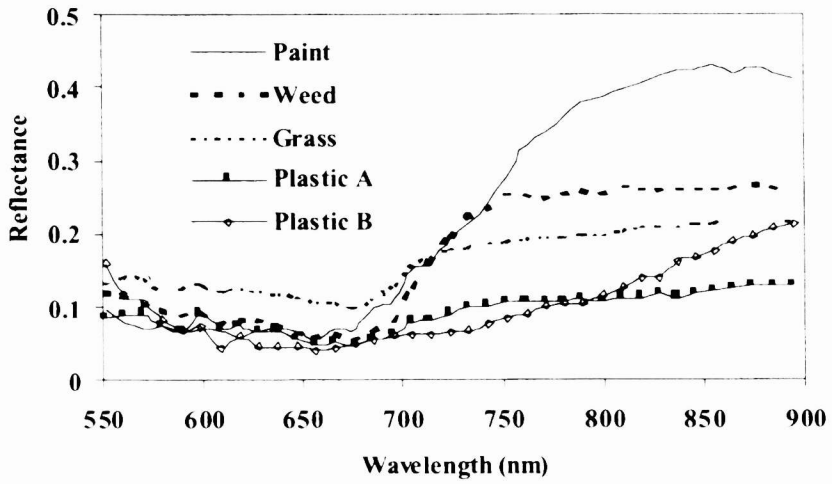

Figure 7: Spectra of selected scene components measured under white-light illumination.

Standard hyperspectral analysis algorithms[3,4] were applied to detect the man-made targets contained in the scene. Supervised classification methods require library spectra as input and make use of spectral distance measures to discriminate between targets and background. One such classification algorithm, Spectral Angle Mapper (SAM), computes the angle in n-dimensional spectral space between a reference spectrum (endmember) and the spectrum of each scene pixel, where n is the number of bands. Pixels are assigned to a given class based on the magnitude of the spectral angle. Since spectral angle is related to the *shape* of the spectrum, SAM is relatively insensitive to variations in illumination that may give a measured spectrum an overall shift in *amplitude*.

Figure 8 shows the cumulative distribution of spectral angle for the painted portions of the scene as well as for the vegetation. The angles given in Figure 8 are relative to the paint-endmember spectrum stored in a previously measured spectral library. The threshold angle is chosen to maximize the number of pixels in the scene classified as paint while minimizing false detections. For example, selecting a threshold angle of 0.13 correctly identifies 70 percent of the paint pixels with no false detections. Additional paint pixels can be detected by increasing the threshold, with a corresponding increase in false detections. Thus, the threshold is a somewhat subjective parameter that will change depending on the scene components as well as on the operational requirements.

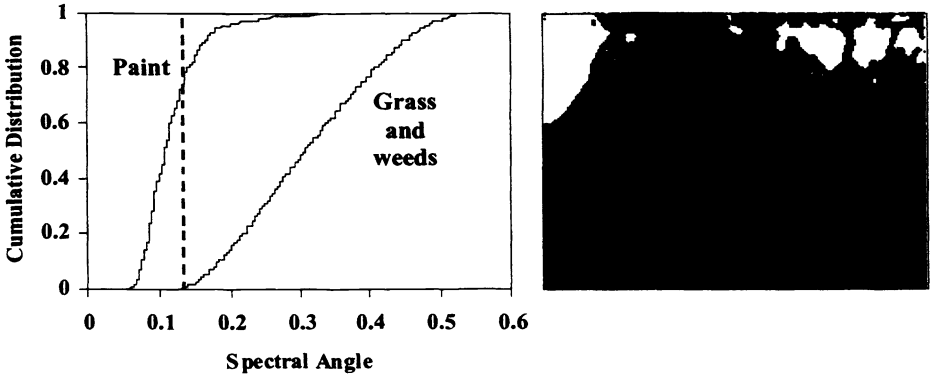

Figure 8: Cumulative distribution of spectral angle for green paint and background, relative to a paint endmember. The bright pixels in the image on the right are those identified as paint using a threshold spectral angle of 0.13.

Similarly, the plastic-B target was detected against vegetation by setting a spectral-angle threshold of 0.2 (see Figure 9).

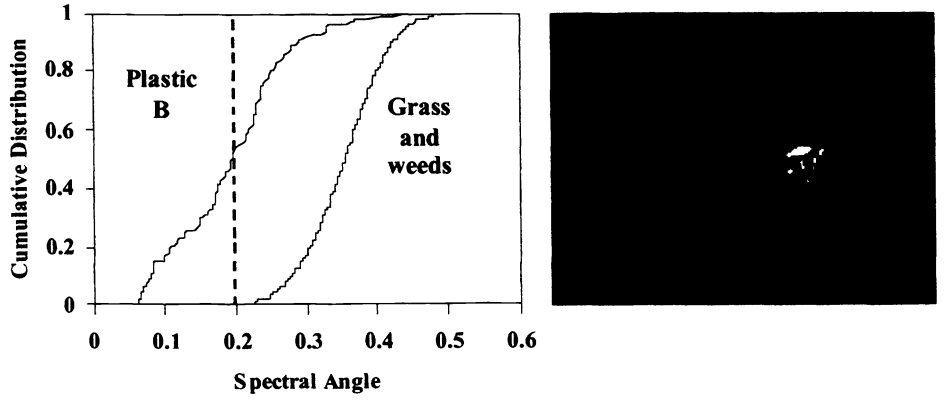

Figure 9: Cumulative distribution of spectral angle for plastic-B and background, relative to a plastic-B endmember. The image on the right shows the plastic-B pixels isolated by setting a threshold of 0.2.

Another classification algorithm, the Minimum Distance (MD) method, computes an Euclidean distance in n-dimensional spectral space between a reference spectrum and the spectrum of each image pixel. Scene pixels are assigned to a given class based on the magnitude of this distance. Figure 10 displays the cumulative distribution of spectral distance from the plastic-A endmember spectrum for all of the plastic-A pixels in the scene as well as for the background vegetation. Since plastic-A is very dark green in color and therefore has a relatively flat spectrum over the 600 to 920-nm range, the MD algorithm provided better separation between plastic-A and the vegetation than did SAM. A distance threshold of 0.42 classifies approximately 40 percent of the plastic-A pixels in the scene correctly with no false detections.

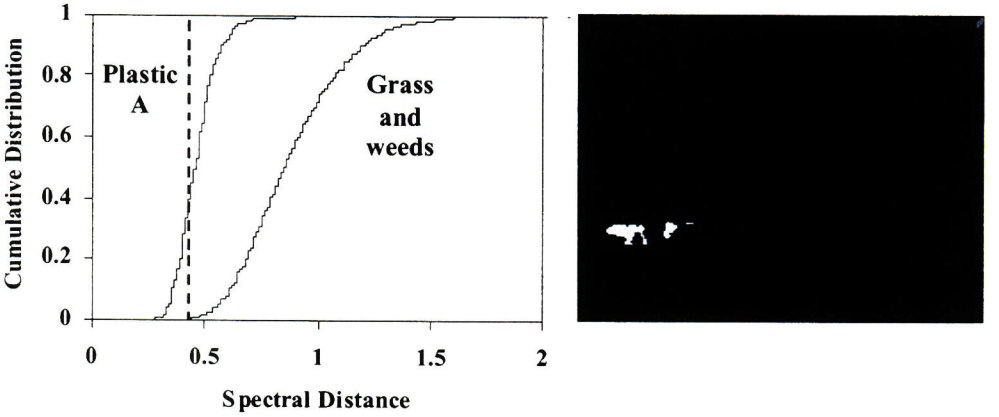

Figure 10: Cumulative distribution of spectral distance for plastic-A and background. The endmember was plastic-A. The image on the right shows the plastic pixels isolated by setting a threshold of 0.42.

3.4 Fusion of Target Detections using Fluorescence, Polarization, and White-Light Reflectance

The fusion of the fluorescence, polarization, and white-light images allowed detection and discrimination of all of the targets in the scene. Figure 11 shows the highlighted target detections resulting from the fusion of the fluorescence, polarization and white-light reflectance imaging. Note that fusion is not simply an overlay of individual detections, but involves some intelligence (which can be automated) in interpreting the target detections. For example, the image in Figure 6 gives some indication that an extended target is evident in the lower right quadrant of the scene. We can use that as a cue to interrogate that section of the scene more fully in the white-light hypercube. When we do so, greater detail is revealed in image data around 600 nm and we can fuse those data with the DOP imagery to reveal an extended copper-colored wire. Thus, the different phenomena exploited by laser illumination can be used to detect different target classes, identify specific targets, reject false detections, and cue each other on scene components of possible interest

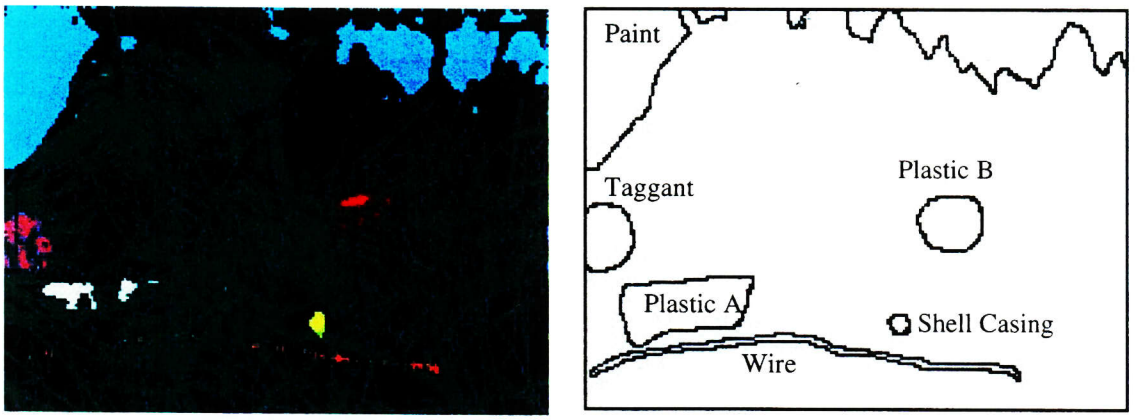

Figure 11: Fused fluorescence, polarization, and reflectance data displayed in one scene and compared to target placement

One of the most important questions that we hope to answer as our program develops is " how many bands are necessary to provide adequate target detection and acceptable false-detection rejection?" It is clear from Figure 7 that the targets and backgrounds examined in this exercise have fairly broad, featureless spectra in the visible through near-IR spectral regions. Thus we would expect that larger spectral bins might offer high detection probability, with a corresponding reduction in processing requirements. We repeated the previous analyses after binning the image cube to 50-nm-wide spectral bins, instead of 10-nm, as was done previously. The spectral angle and distance separations achieved using the resulting seven spectral bands were comparable to those computed using the 33-band, 10-nm data. Thus, although our system collects hyperspectral data, we recognize that not all targets and background will require high-spectral resolution analysis, especially when examining only their visible to near-infrared reflectance features. We postulate, for example, that at longer infrared wavelengths, hyperspectral imaging may become necessary to distinguish targets with similar visible-reflectance characteristics (such as camouflage). Clearly, phenomenology measurements on a variety of targets and backgrounds will aid us in selecting the number and width of spectral bands appropriate for a given application.

4. FUTURE SYSTEM DEVELOPMENT

The baseline system has demonstrated the potential utility of active illumination in enhancing target detectability and identification. Even in its current form, it could provide a useful adjunct sensor for either cueing or identifying landmines in a variety of environmental conditions. However, in order to explore the full utility of active hyperspectral imaging, we are currently developing a short-wave infrared (SWIR) hyperspectral system that will extend the spectral coverage of our baseline system out to 2 μm. Active illumination in the 1 to 2-μm region offers several potential advantages, especially in a tactical scenario. First, the spectral reflectivity of many paints and fabrics, as well as of certain vegetation, has more structure in the SWIR region and, thus, detection may be facilitated. Second, for wavelengths above 1.5 μm, the illuminator is eyesafe at even close ranges, which is an important practical consideration. Finally, the SWIR system will be largely covert, since focal plane arrays sensitive to that spectral region are not common field instruments.

We have recently fabricated the SWIR white-light laser, using the same architecture as was used in the visible/NIR version. A 1.064-μm microlaser (10 μJ per pulse) is focused into a 100-m silica fiber, which results in a broad continuum of radiation extending from about 0.85 μm to 2.25 μm (see Figure 12). In the SWIR white-light laser, a number of different nonlinear interactions occur so that the continuum commences fairly close to the pump wavelength, without the noticeable Stokes lines evident in the visible device. These interactions include stimulated Raman scattering, as before, but also self and cross phase modulation, and four-wave mixing. The resultant output of the SWIR white-light laser is considerably more "filled-in" compared to the visible device and includes output at wavelengths shorter than the pump (due to four-wave mixing).

The SWIR AHSI system will comprise the SWIR white-light source and an acousto-optic tunable filter (AOTF)-based dispersion element coupled to a cooled InSb focal-plane array. In contrast to the scanning visible system, the SWIR system will be staring, where high-resolution spatial data will be acquired in each of approximately 75 spectral bands. We chose this combination of components in order to develop as compact a system as possible, as well as to compare scanning versus staring operation. We expect to be acquiring data with this system in the spring of 1999.

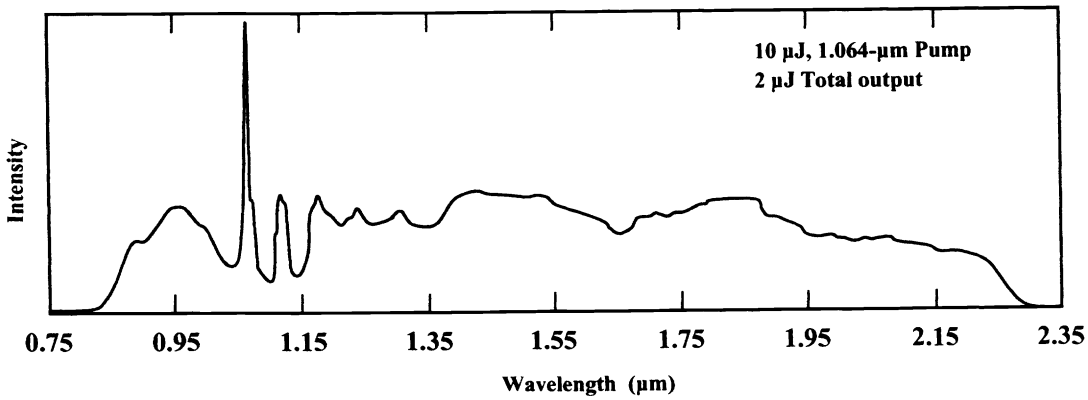

Figure 12: Measured output spectrum of SWIR white-light source.

In addition to developing and testing SWIR active hyperspectral components, we are also exploring ways in which broadband mid-wave infrared (MWIR) sources can be fabricated and incorporated into a hyperspectral–imaging system. In the MWIR, nominally 3 to 5 μm in wavelength, hyperspectral imagers view emitted as well as reflected radiation and it is not clear when active illumination provides an operational advantage over passive. One of our program objectives is to conduct the phenomenology measurements to address that question and to use the results of those measurements to design application-specific laser and imaging systems.

Finally, we have already begun to explore fusion of the visible/NIR hyperspectral imagery with long-wave infrared (LWIR) thermal imagery. Since the target signatures at LWIR wavelengths (8 to 12 μm) result from emission, there seems to be little justification for developing a broadband source in that region. We have, however, been exploring enhancement of thermal signatures using microwave irradiation. This technique shows particular promise for the difficult task of detecting plastic mines in soil or in vegetatively cluttered environments. As an example, we have recently set up a complex target scene consisting of surface exposed, obscured, and buried plastic objects. The spectral reflectivity of the surface targets was analyzed to distinguish plastics from like-colored vegetation. We then heated the entire target scene in a household microwave oven (~ 1 kW) for 5 seconds and viewed the scene with an inexpensive thermal imager. Buried plastic objects are easily discernible because of the differential heating induced by the microwave radiation. We are continuing to explore this technique and will be reporting on the results in the near future.

5. SUMMARY

We have assembled and tested an active hyperspectral imaging system comprising a microlaser-based illuminator that emits from 532 to 900 nm, and a scanning imaging spectrometer. We have tested this system on a number of target scenes, both indoors and outdoors, and have developed a suite of processing tools useful for discrimination of targets in highly-cluttered backgrounds. In this paper, we have presented one example target scene and demonstrated the utility of fluorescence imaging, polarimetry, and white-light reflectance in detecting and identifying targets with a minimum of false detections. Although we still have much data to acquire in order to derive useful statistics on the technique, our early results are encouraging.

We are also developing systems that expand the wavelength coverage to include the SWIR , MWIR, and LWIR bands, and to develop fusion algorithms to exploit the full capability of such broad spectral coverage. We have focussed on developing systems that are compact and thus amenable to deployment from a vehicle, UAV, or even man-portable. In summary, we believe that active hyperspectral imaging systems have the potential to provide an unparalleled level of target discrimination for a large variety of applications and we will continue to acquire data to explore their potential.

ACKNOWLEDGEMENTS

The work presented in this paper was sponsored under Air Force Contract number F19628-95-C-0002. Opinions, interpretations, conclusions, and recommendations are those of the authors and are not necessarily endorsed by the United States Air Force.

REFERENCES

1. J. J. Zayhowski and C. Dill III, Opt. Lett. **18**, 1427 (1994).
2. J. J. Zayhowski, Laser Focus World **April** (1996).
3. J.R. Schott, *Remote Sensing: The Image Chain Approach,* Oxford University Press, New York, 1997.
4. R. A. Schowengerdt, *Remote sensing, models, and methods for image processing, 2nd ed.* Academic Press, San Diego, 1997.